Nonlinear charge and current neutralization of an ion beam pulse in a pre-formed plasma

Igor D. Kaganovich,[a] Gennady Shvets, Edward Startsev, and Ronald C. Davidson
Plasma Physics Laboratory, Princeton University, Princeton, New Jersey 08543

(Received 22 February 2001; accepted 30 May 2001)

The propagation of a high-current finite-length ion beam in a cold pre-formed plasma is investigated. The outcome of the calculation is the quantitative prediction of the degree of charge and current neutralization of the ion beam pulse by the background plasma. The electric and magnetic fields generated by the ion beam are studied analytically for the nonlinear case where the plasma density is comparable in size with the beam density. Particle-in-cell simulations and fluid calculations of current and charge neutralization have been performed for parameters relevant to heavy ion fusion assuming long, dense beams with length $l_b \gg V_b/\omega_b$, where V_b is the beam velocity, and ω_b is the electron plasma frequency evaluated with the ion beam density. An important conclusion is that for long, nonrelativistic ion beams, charge neutralization is, for all practical purposes, complete even for very tenuous background plasmas. As a result, the self-magnetic force dominates the electric force and the beam ions are always pinched during beam propagation in a background plasma. © *2001 American Institute of Physics.* [DOI: 10.1063/1.1386804]

I. INTRODUCTION

Understanding the transport of charged particle beams in background plasma is important for fundamental physics as well as for a variety of applications. As early as 1939,[1,2] it was pointed out that the transport of cosmic rays may be governed by the charge and current neutralization by the ambient plasma. The recent resurgence of interest in charged particle beam transport in background plasma has been brought about by the suggestion that the plasma can be used as a magnetic lens. Applications of the plasma lens, ranging from heavy ion fusion to high-energy lepton colliders, are discussed in Refs. 3–10. In particular, both heavy ion fusion and high-energy physics applications involve the transport of *positive* charges in plasma: partially stripped heavy elements for heavy ion fusion; positrons for electron–positron colliders;[9] and high-density laser-produced proton beams for the fast ignition of inertial confinement fusion targets. The emphasis of the present work on positive ions is deliberate because, as we demonstrate below, the transport of positive ion beams through background plasma is very different from that of the negatively charged beams. A beam of positively charged particles attracts plasma electrons into the beam, whereas a beam of negative charges repels the electrons out of its path. An important consequence, which is one of the findings of the present calculation, is that a nonrelativistic positive ion beam with density n_b can be neutralized to a very high degree by a large-volume tenuous plasma with ambient density $n_p \ll n_b$.

The beam charge and current neutralization by plasma electrons is an important issue for beam propagation in a background plasma. Beam focusing schemes rely on complete charge neutralization and partial current neutralization for magnetic focusing in plasma lenses,[5] and for ballistic ion focusing in heavy ion fusion.[8] In these applications, the plasma is pre-formed by an external plasma source and is independent of the beam characteristics.

The goals of the present calculation are: (a) to derive a system of reduced equations for the electric and magnetic field generated by an ion beam propagating through background plasma, and (b) to develop a semianalytical method for robust and easy assessment of the effects of these fields on the beam transport. The case where the beam propagates through a cold unmagnetized plasma, with plasma density large compared with the beam density, can be studied by use of linear perturbation theory.[3,4] The transport of relativistic electron beams has been studied in detail in various contexts.[4–6,11] The transport of a stripped pinched ion beam has been also discussed in Ref. 8, where the assumption of current neutrality was made to determine self-consistent solutions for the electric and magnetic fields. Here, we focus on the nonlinear case where the plasma density has an arbitrary value compared with the beam density, and correspondingly, the degree of current neutralization is arbitrary. For simplicity, we neglect transient effects at the plasma boundary during beam entry into the plasma. At first we assume steady-state properties in the frame of the beam, and then generalize the results for variable shape ion beams. Rosenbluth *et al.*[12] have considered the equilibrium of an isolated, charge-neutralized, self-pinched ion beam pulse, in the absence of background plasma. In contrast, we consider the case where ''fresh'' uniform plasma is always available in front of the beam.

To simplify the analysis and make the problem tractable, a number of assumptions have been made. First, we neglect the dynamics of the beam ions and plasma ions. The beam ions are assumed to be moving in the z direction with constant axial velocity V_b. The response time of the plasma ions is determined by the ion plasma frequency, which is much

[a]Electronic mail: ikaganov@pppl.gov

longer than the electron response time. Therefore, neglecting the dynamics of the plasma ions is well justified. Second, the entrance of the beam into the plasma will not be addressed in the present model. Furthermore, beam ionization effects are neglected, and the background plasma in front of the beam is assumed to be uniform and stationary. As a result, all field quantities (electric and magnetic), and the plasma and beam charge densities and current densities are stationary in a reference frame moving axially with the beam.

Additional simplifications of the electron fluid equations are possible for long beams where the beam half length (l_b) is much longer than both the beam radius (r_b) and the plasma neutralization length, which is equal to the ratio of the beam velocity (V_b) to the electron plasma frequency (ω_p). The first assumption is used in the Darwin model.[13] The second assumption allows further simplifications. We show that under these conditions a reduction of the dimensionality of the problem is possible. For an axisymmetric beam, the longitudinal electron flow velocity is determined by a one-dimensional equation in the radial direction for each axial slice of the beam. Furthermore, we show that this equation holds not only for steady-state ion beams profile but also for slowly varying compared to electron plasma frequency profiles. Once the longitudinal electron flow velocity is determined, the electric and magnetic fields can be calculated from simple analytical expressions.

As an application of the theoretical model, we study transport of the ion beam pulse in the target chamber for heavy ion fusion. At the present time, the main approach to heavy ion fusion is ballistic focusing in the target chamber from an initial beam radius of about 3 cm down to a spot size of about 3 mm. The beam traverses the chamber (radius about 3 m), in near vacuum (a few mTorr of flibe vapor). Typical beam parameters are:[8] Cs^+ ions with energy 2.5 GeV, beam velocity $V_b \approx 0.2c$, beam current $\approx 4kA$, and main pulse duration 10 ns. The beam ion density range is $10^{11}-10^{13}\,\mathrm{cm}^{-3}$, depending on the beam radius, providing space-charge potentials of a few MV. This large ion space charge is to be neutralized by a background plasma. The plasma can be created in the chamber by an external plasma source, by gas ionization by the beam ions, and by photoionization from the target, which is bombarded by beam ions preceding the main pulse. Both electrostatic defocusing and magnetic pinching of the beam have to be avoided for controlled ballistic focusing. Thus large self-electric and self-magnetic fields have to be avoided during focusing of the ion beam pulse. Since the beam parameters vary significantly for different heavy ion fusion scenarios, analytical results are of considerable importance for parametric studies, benchmarking of numerical codes, and comparison with experiments.

II. BASIC EQUATIONS FOR DESCRIPTION OF ION BEAM PULSE PROPAGATION IN A PLASMA

We consider all equations in the reference frame of the laboratory plasma. The plasma ion response time is assumed to be large compared with the beam pulse duration, and, therefore, the background plasma ion density remains uniform during beam propagation. The beam density profile is also assumed to be given. The plasma electron density n_e, however, is a function of both the unperturbed plasma density n_p, and the ion beam density profile. The plasma electrons are assumed to be cold, and electron thermal effects are neglected. This approach has been widely used to study laser-plasma interactions.[4,5,11] These assumptions are well justified for ion beam pulses envisioned for heavy ion fusion.

The electron fluid equations together with Maxwell's equations comprise a complete system of equations describing the electron response to a propagating ion beam pulse. The electron fluid equations consist of the continuity equation

$$\frac{\partial n_e}{\partial t}+\nabla\cdot(n_e\mathbf{V}_e)=0, \tag{1}$$

and the force balance equation

$$\frac{\partial \mathbf{p}_e}{\partial t}+(\mathbf{V}_e\cdot\nabla)\mathbf{p}_e=-e\left(\mathbf{E}+\frac{1}{c}\mathbf{V}_e\times\mathbf{B}\right), \tag{2}$$

where $-e$ is the electron charge, m is the electron rest mass, $\mathbf{V}_e$ is the electron flow velocity, $\mathbf{p}_e=\gamma_e m\mathbf{V}_e$ is the electron momentum, and $\gamma_e=1/\sqrt{1-V_e^2/c^2}$ is the relativistic mass factor. Maxwell's equations for the self-generated electric and magnetic fields, $\mathbf{E}$ and $\mathbf{B}$, are given by

$$\nabla\times\mathbf{B}=\frac{4\pi e}{c}(Z_b n_b\mathbf{V}_b-n_e\mathbf{V}_e)+\frac{1}{c}\frac{\partial\mathbf{E}}{\partial t}, \tag{3}$$

$$\nabla\times\mathbf{E}=-\frac{1}{c}\frac{\partial\mathbf{B}}{\partial t}, \tag{4}$$

where $\mathbf{V}_b$ is the ion beam velocity, n_e and n_b are the number densities of the plasma electrons and beam ions, respectively, and Z_b is the ion beam charge state.

Considerable simplification can be achieved by applying the conservation of generalized vorticity. Indeed, operating on the electron momentum equation (2) with $\nabla\times$, and making use of Eq. (4), we obtain the equation for the generalized vorticity $\mathbf{\Omega}=\nabla\times\mathbf{p}_e-e\mathbf{B}/c$, i.e.,

$$\frac{\partial\mathbf{\Omega}}{\partial t}-\nabla\times(\mathbf{V_e}\times\mathbf{\Omega})=0,$$

which can be rewritten in the form

$$\frac{\partial\mathbf{\Omega}}{\partial t}+(\mathbf{V_e}\cdot\nabla)\mathbf{\Omega}=-\mathbf{\Omega}(\nabla\cdot\mathbf{V_e})+(\mathbf{\Omega}\cdot\nabla)\mathbf{V_e}. \tag{5}$$

Equation (5) shows that the generalized vorticity is transported along with the electrons and that the source term is proportional to the generalized vorticity. It can be shown from Eq. (5) that if $\mathbf{\Omega}=0$ everywhere at some initial time, then it continues to vanish at all subsequent times. This is the class of solutions (with $\mathbf{\Omega}=0$) examined in the present paper. (An additional discussion is presented in Appendix B.) For example, if the generalized vorticity $\mathbf{\Omega}$ is initially equal to zero ahead of the beam, and all streamlines inside of the beam originate from the region ahead of the beam (where $\mathbf{\Omega}=0$), then $\mathbf{\Omega}$ remains equal to zero everywhere. In the general case, there may exist solutions where $\mathbf{\Omega}\neq 0$ at some locations within the beam, and the streamlines originating

from the region ahead of the beam pass around these regions. This class of solutions is not treated in the present paper. In the absence of background plasma, an example of a solution with $\mathbf{\Omega}\neq 0$ inside the beam has been examined by Rosenbluth *et al.*[12] The interaction of solutions with $\mathbf{\Omega}\neq 0$ with background plasma will be the subject of future study.

Thus the magnetic field, $\mathbf{B}$, is related to the electron flow velocity, $\mathbf{V}_e$, by

$$\mathbf{B}=\frac{c}{e}\nabla\times\mathbf{p}_e, \tag{6}$$

which has the form of the London equation for superconductivity.[14] Note that Eq. (6) is an exact result, and is not obtained under linearization assumptions. Making use of the London equation (6), the electron momentum equation (2) simplifies to become

$$\frac{\partial\mathbf{p}_e}{\partial t}+\nabla(K_e)=-e\mathbf{E}, \tag{7}$$

where $K_e=\gamma_e mc^2$ is the electron energy. For laser–plasma interactions, the hydrodynamic equations in this form were displayed in Ref. 14.

Note that the inertia terms in Eq. (2) are comparable in size to the Lorentz force term and cannot be omitted. Estimating the magnetic field from Eq. (6), one concludes that the electron gyroradius, $\rho_e=V_{ez}mc/eB$, is of order the beam radius. This is a consequence of the fact that the electrons originate from the region of zero magnetic field in front of the beam. If most electrons are dragged along with the beam and originate from the region of large magnetic field, the situation may be different.[12]

III. APPROXIMATE SYSTEM OF EQUATIONS FOR LONG BEAMS

A. Steady-state ion beams

The formalism in this section is restricted to the assumption that all quantities are stationary in the reference frame of the moving beam, i.e., all quantities depend on t and z exclusively through the combination

$$\zeta=V_b t-z. \tag{8}$$

Moreover, the analysis is carried out in the laboratory frame of reference, where the transformation of derivatives is

$$\left(\frac{\partial}{\partial t}\right)_z=V_b\frac{\partial}{\partial\zeta},\quad \left(\frac{\partial}{\partial z}\right)_t=-\frac{\partial}{\partial\zeta}. \tag{9}$$

In this section, an approximate set of equations is derived for a long, cylindrically symmetric beam satisfying

$$l_b\gg V_b/\omega_p,\quad l_b\gg r_b, \tag{10}$$

where $\omega_p=(4\pi e^2 n_e/m)^{1/2}$ is the electron plasma frequency. We also assume that the fields and electron flow velocity and density are in steady-state in the reference frame moving with the beam. The electron flow velocity is found by substituting Eq. (6) into the $\nabla\times\mathbf{B}$ Maxwell equation (3), which yields

$$-\frac{1}{r}\frac{\partial}{\partial r}\left[r\left(\frac{\partial p_{ez}}{\partial r}+\frac{\partial p_{er}}{\partial\zeta}\right)\right]=\frac{4\pi e^2}{c^2}(Z_b n_b V_b-n_e V_{ez})+\frac{eV_b}{c^2}\frac{\partial E_z}{\partial\zeta}. \tag{11}$$

For long beams with $l_b\gg V_b/\omega_p$, the displacement current [the final term on the right-hand side of Eq. (11)] is of order $(V_b/\omega_p l_b)^2\ll 1$ compared with the electron current. Because $l_b\gg r_b$ is assumed, the second term on the left-hand side of Eq. (11) is of order $(r_b/l_b)^2(\ll 1)$ smaller than the first term on the left-hand side. As we shall prove below, the electron flow velocity does not approach ultrarelativistic values even for $\beta_b\to 1$, therefore, ultrarelativistic electron effects are not important.

For sufficiently long beams [Eq. (10)], the system of nonstationary two-dimensional equations (1)–(4) reduces to a one-dimensional equation for the longitudinal electron flow velocity V_{ez}, and Eq. (11) can be approximated by

$$-\frac{1}{r}\frac{\partial}{\partial r}\left[r\left(\frac{\partial p_{ez}}{\partial r}\right)\right]=\frac{4\pi e^2}{c^2}(Z_b n_b V_{bz}-n_e V_{ez}), \tag{12}$$

where V_{bz} is the z-component of the ion beam mean velocity, and the subscript z is inserted to emphasize the fact that longitudinal electron flow velocity is entirely determined by the longitudinal ion current $Z_b e n_b V_{bz}$. As a consequence of Eq. (10), both the electron and ion radial velocities are negligibly small compared with the corresponding longitudinal velocities. This is reflected by Eq. (12), which states that the electron motion is determined by the longitudinal ion current. Note that Eq. (12) is valid in the nonlinear regime for arbitrary values of the plasma density. Equation (12) shows that the degree of current neutralization is determined by the ratio of the beam radius r_b to the skin depth c/ω_p, similar to what is found in linear theory (see, for example, Ref. 3). If $r_b\gg c/\omega_p$, the ion current is well neutralized by the electron return current, i.e., the longitudinal electron velocity is reciprocal to the plasma density ($V_{ez}=Z_b V_b n_b/n_e$) and is small for the plasma density much larger than the beam density. The net current in the beam region can be estimated from Eq. (12) as

$$I_{\rm net}=\pi e\int_0^{r_b}(Z_b n_b V_b-n_e V_{ez})r\,dr=\frac{c^2 r_b}{4\pi e}\left(\frac{\partial p_{ez}}{\partial r}\right)_{r_b}\simeq\beta_b Z_b\frac{mc^3}{4e}\frac{n_b}{n_e}\frac{r_b}{\delta}=4.25\beta_b Z_b\frac{n_b}{n_e}\frac{r_b}{\delta}kA, \tag{13}$$

where δ is the characteristic scale length of the electron longitudinal momentum derivative. In the case of a smooth profile for $n_b(r)$, $\delta\sim r_b$, whereas in the case of a step-function profile, $\delta\sim c/\omega_p$.

In the opposite limit ($r_b\ll c/\omega_p$), the ion beam current is not neutralized, and the electron longitudinal velocity is determined entirely by the ion beam current and does not depend on the plasma density.

The radial electron flow velocity may be determined from the electron continuity equation (1). We obtain

$$V_{er}=-\frac{1}{rn_e}\frac{\partial}{\partial\zeta}\int_0^r[n_e(V_b-V_{ez})-n_pV_b]rdr, \tag{14}$$

where n_p is the uniform background plasma density without the beam present. The constant n_pV_b has been added under the integral in Eq. (14) to make the term in brackets zero when the beam is absent. If quasineutrality is assumed, $n_e(V_b-V_{ez})-n_pV_b=(n_e-n_p)V_b-n_eV_{ez}=Z_bn_bV_b-n_eV_{ez}\equiv j_z/e$, and Eq. (14) simplifies to become

$$V_{er}=-\frac{1}{ern_e}\frac{\partial}{\partial\zeta}\int_0^r j_zrdr, \tag{15}$$

where $j_z=e(Z_bn_bV_b-n_eV_{ez})$ is the longitudinal current. Equation (14) is a consequence of $\nabla\cdot\mathbf{j}=0$. The radial electron velocity is of order $(V_b-V_{ez})r_b/l_b$, and is small compared with the beam velocity V_b. Substituting V_{er} and V_{ez} into Eq. (7) then yields the electric field

$$\mathbf{E}=-\frac{1}{e}\left(V_b\frac{\partial\mathbf{p}_e}{\partial\zeta}+\nabla K_e\right). \tag{16}$$

Substituting V_{er} and V_{ez} into Eq. (6) yields the azimuthal magnetic field

$$B=-\frac{c}{e}\left(\frac{\partial p_{ez}}{\partial r}+\frac{\partial p_{er}}{\partial\zeta}\right). \tag{17}$$

As can be seen from Eqs. (16) and (17), the values of electric and magnetic fields are strongly reduced in the case of dense plasma ($r_b\gg c/\omega_p, n_p\gg n_b$) where the electron flow velocity is much smaller than the beam velocity.

Finally, the degree of charge neutralization can be estimated directly from Poisson's equation

$$\rho=\frac{1}{4\pi}\nabla\cdot\mathbf{E}, \tag{18}$$

where $\rho=e(Z_bn_b-n_e)$. Using Eqs. (12), (16), and (18) it can be shown that the maximum deviation from quasineutrality occurs when $r_b\sim c/\omega_p$, and

$$|\rho|\lesssim e\beta_b^2Z_bn_b. \tag{19}$$

Therefore, for nonrelativistic long ion pulses, $|\rho|/eZ_bn_b\ll 1$ and there is almost complete charge neutralization. For calculational purposes, exact charge neutralization,

$$n_e=Z_bn_b+n_p, \tag{20}$$

can be assumed and deviations from quasineutrality can be calculated from Eq. (18) in a subsequent iteration. Section IV provides more quantitative estimates.

The radial force acting on the beam ions can also be determined in terms of the electron flow velocity. Substituting Eqs. (16) and (17) into the ion force equation yields

$$F_r=eZ_b\left(E_r-\frac{1}{c}V_bB\right)=-Z_b\frac{\partial}{\partial r}(K_e-V_bp_{ez}). \tag{21}$$

Because the radial flow velocity is small compared with the longitudinal flow velocity for long beams, it can be neglected in Eq. (21), which simplifies to become

$$F_r=Z_bm\gamma_e^3(V_b-V_{ez})\frac{\partial}{\partial r}V_{ez}. \tag{22}$$

Equation (22) was derived in Ref. 8 in nonrelativistic form. Because $V_{ez}<V_b$, and because V_{ez} is a monotonically decreasing function of radial coordinate r (if $Z_bn_bV_b$ is a monotonically decreasing function of radial coordinate r), the radial force in Eq. (22) acting on the beam ions is always inward ($F_r<0$), i.e., it pinches the ion pulse. The radial force in Eq. (22) is greatly reduced for $V_{ez}\simeq V_b$, which corresponds to the case of good current neutralization, and background plasma density small compared to the beam density. The value of radial force acting on the beam ions is strongly reduced in the case of dense plasma ($r_b\gg c/\omega_p, n_p\gg n_b$) where the electron flow velocity is much smaller than beam velocity.

B. Variable shape ion beams

In applications where the ion beam profiles are not stationary, n_b is not only a function of (ζ,r) but also t. In this case the introduction of the variable ζ is inadequate, and we use the laboratory frame coordinates (r,z,t). For example, in reactor designs for heavy ion fusion, the ion beams converge to smaller radial size during ballistic focusing. Nevertheless, if the beam profile variations are slow compared to the electron plasma frequency, many of the results for stationary beams can be applied. First of all, if the ion beam propagates in a preformed plasma, the generalized vorticity is conserved even for a nonstationary beam, and the London equation (6) is valid. Because the assumptions in Eq. (10) are valid for long, slowly varying beams, Eq. (12) can be used for estimating the longitudinal electron flow velocity. Also because the radial velocity is much smaller than the longitudinal velocity for long beams, the electric field can be determined from Eq. (7) making use of the time-dependent p_{ez} obtained from Eq. (12). The space-charge density can be determined from Poisson's equation (18). As discussed above, nonrelativistic, long, slowly varying ion beams are well charge neutralized. Thus, the radial electron flow velocity may be obtained from the quasineutrality condition $\nabla\cdot\mathbf{j}=0$, which gives

$$V_{er}=\frac{1}{en_e}\left(\frac{1}{r}\int_0^r\frac{\partial j_z}{\partial z}rdr+j_{br}\right). \tag{23}$$

Here, $j_z=e(Z_bn_bV_{bz}-n_eV_{ez})$ is the longitudinal current, and $j_{br}=eZ_bn_bV_{br}$ is the radial beam current. The system of Eqs. (6), (7), (12), (18), and (23) yield a complete system of equations describing long, slow-varying ion beams. In summary, the only qualitatively new features which emerge for nonstationary ion beams are two new terms appearing in Eq. (7) and in Eq. (23). These correspond to the time derivative of the longitudinal momentum in Eq. (7), describing the effects of ion beam density variation, and the effects of radial beam current on the radial electron velocity, described by the last term on the right-hand side of Eq. (23). Examples of detailed simulations are given in the next section.

IV. EXAMPLES OF CALCULATIONS FOR HEAVY ION FUSION PARAMETERS

We have performed self-consistent calculations of the electric and magnetic fields and the electron flow velocity according to Eqs. (13)–(16). In the first iteration, complete charge neutrality (20) is assumed. The corrections, including small departures from quasineutrality and the effects of displacement current and radial components of velocity [Eq. (11) compared to Eq. (12)], are then obtained in the second iteration. The electron velocity does not approach ultrarelativistic values even for $\beta_b \to 1$, and therefore, ultrarelativistic electron effects are not important.

A. Ion beam at the entrance of the target chamber for heavy ion fusion

Typical results of the calculations are shown in Fig. 1. The characteristic parameters of the ion beam pulse are: singly charged Cs^+ ions; ion energy $E_b = 4$ GeV ($\beta_b = 0.25$); maximum (in the middle section of the beam) ion current $I_b = 4$ kA ($n_b = 1.2 \times 10^{11}\,\mathrm{cm}^{-3}$); maximum beam radius $r_b = 3$ cm; half-length $l_b = 40$ cm; and background plasma density $n_p = 10^{11}\,\mathrm{cm}^{-3}$. The ion pulse is formed in the drift compression region of the accelerator and is assumed to have a density distribution corresponding to the self-similar solution in the drift compression region, i.e., a uniform ion density up to radius $r(z) = r_b\sqrt{1-(z/l_b)^2}$,[15] and zero density for larger radius [Fig. 1(a)]. For the conditions in Fig. 1, the plasma density is chosen to be comparable to the ion beam density. The skin depth is assumed to be smaller than the beam radius, so the beam current is neutralized, and the longitudinal electron velocity is $V_{ez} \simeq V_b n_b/(n_p + n_b)$ in the beam region, and decays exponentially outside the beam over distances of order the skin depth [Fig. 1(b)]. The current is neutralized in the beam center up to about 80%, and because the electron flow velocity is monotonically decreasing with radial coordinate r [Fig. 1(b)], the degree of current neutralization decreases towards the beam edge and approaches 50% at the boundary. Note that this estimate is consistent with Eq. (13), $I_{\mathrm{net}} \approx 1$ kA in the beam center, which is 20% of the beam current (4 kA). If Z_b is increased by stripping, n_e will also rise and I_{net} will remain at about 1 kA (for $Z_b n_b \sim n_e$), while the current neutralization fraction will increase towards 100%. Outside the beam, only the electron return current is present, and therefore, the current is negative [Fig. 1(c)].

The longitudinal electric field E_z is located mainly in front and in back of the beam to accelerate and decelerate electrons to the velocities required to assure that the electron return current neutralizes the ion beam current. Consequently, the longitudinal electric field E_z is of order $mV_{ez}^2/(el_b)$ [Fig. 1(d)]. This electric field is small compared to the electric field of an unneutralized ion beam, and correspondingly the charge neutralization is close to unity (typically about 98% in the head and tail of the beam in the regions of large gradients, and about 99.5% in the main body of the beam). The radial flow velocity calculated from Eq. (15) is depicted in Fig. 1(e). As the beam enters the plasma, the integral $\int_0^r j_z r dr$ increases, and the radial flow velocity is negative, i.e., the beam attracts the background plasma electrons. Further from the beam head, the current neutralization is better, and $\int_0^r j_z r dr$ decreases and the radial flow velocity is positive.

The radial electric field is calculated from the Eq. (16). Relativistic effects are not important for the conditions of Fig. 1, and the radial flow velocity is much smaller than the longitudinal velocity. Therefore, the radial electric field is determined approximately from $E_r \approx -m/(2e)\,(\partial V_{ez}^2/\partial r) > 0$, which is positive in the beam region [Fig. 1(f)]. Similarly, from Eq. (17), the magnetic field is $B \approx -(cm/e)(\partial V_{ez}/\partial r)$, and is shown in Fig. 1(g). Correspondingly, the longitudinal flow velocity is $V_{ez} \approx cE_r/B$. The situation is different in the radial direction, because the inertia and Lorentz force terms are comparable in size in the longitudinal projection of the momentum balance equation (2), and therefore, $V_{er} \neq cE_z/B$. The radial force acting on the beam ions is always negative as discussed above [Fig. 1(h)].

B. Variation of electromagnetic fields in the beam for different plasma densities

Figure 2 depicts the longitudinal electron velocity and the electron streamlines for similar conditions to Fig. 1, but for much smaller background plasma density (hundred times smaller). Under these conditions, the skin depth is much larger than the beam radius (5.6 times larger) outside the beam. Therefore, the electron velocity decays slowly outside the beam over distances of order the skin depth [Fig. 2(a)]. Correspondingly, there is a sizeable radial electric field at distances much larger than the beam radius [Fig. 2(b)]. Although the background plasma density is hundred of times smaller than the beam density, note that it effectively neutralizes both the beam current and charge. Because the electron longitudinal velocity is comparable in both cases [$n_p \sim n_b$ in Fig. 1(b) and $n_p \ll n_b$ in Fig. 2(a)], the electric fields are comparable for both cases and the space charge is similar. Therefore, in the region inside the beam the degree of fractional charge nonneutralization, $f = \rho/(en_b)$, is small according to Eq. (19); however, in the region outside the beam, on distances of order the skin depth, the fields and space charge are of the same order as inside the beam, but the plasma density is much smaller, so the space charge may become comparable to the background charge density, as it does for the conditions in Fig. 2. In this case, strong plasma waves, neglected in the present model, may be excited at the head of the beam. Note that for the conditions in Fig. 2 the radial flow velocity is comparable with the longitudinal velocity at the very beginning of the head, and the one-dimensional model in Eq. (12) does not provide an accurate description of the beam head. The establishment and stability of this profile requires a more detailed investigation, which will be addressed in future publications.

In Fig. 3, the longitudinal electron flow velocity, azimuthal magnetic field, radial electric field, and radial force acting on the beam ions are shown at the midplane of the beam pulse for three values of plasma density. In a dense plasma ($n_p \gg n_b$), the electron velocity $\mathbf{V}_e$ is inversely proportional to the plasma density, in order to support the same

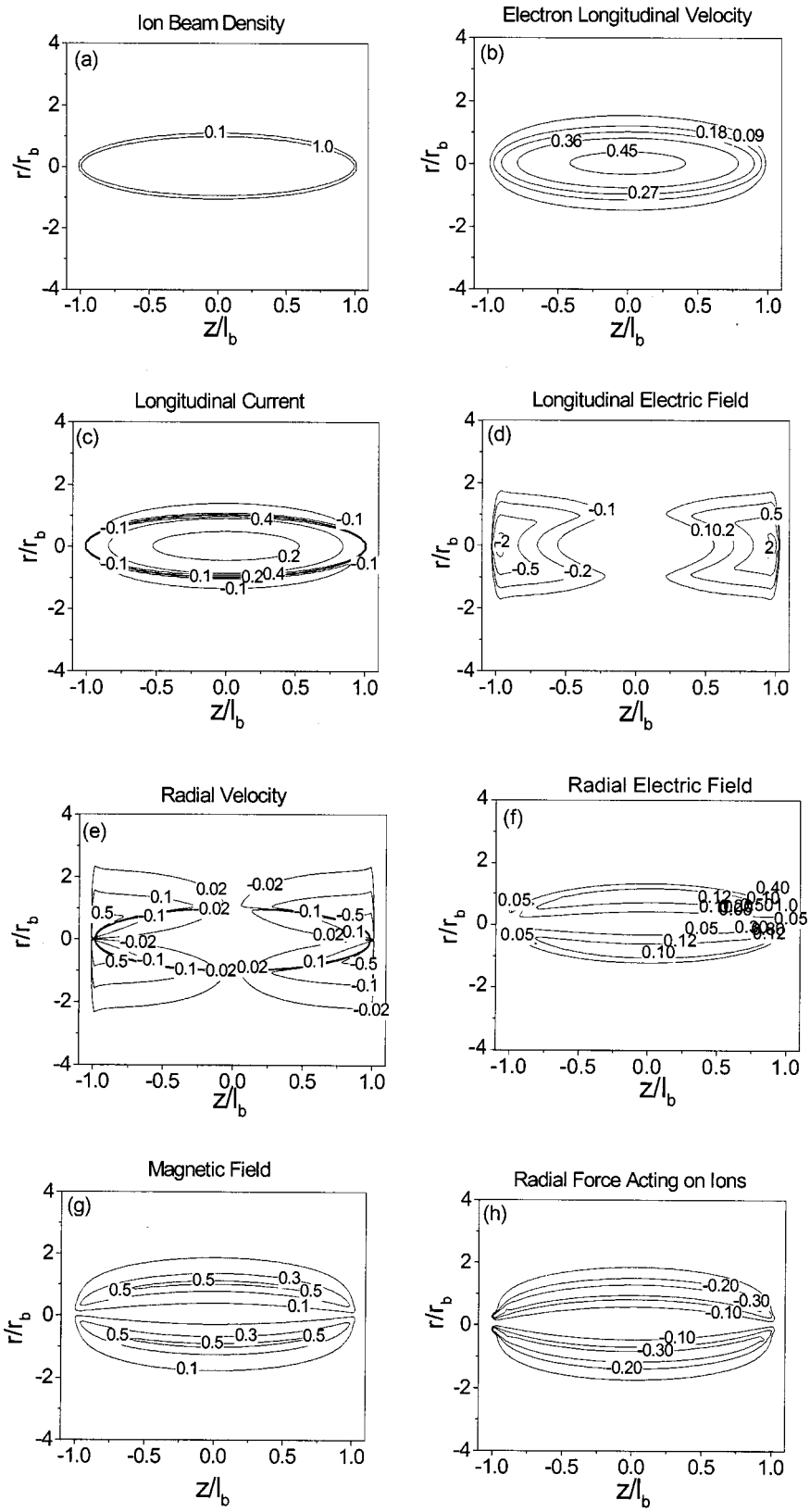

FIG. 1. Characteristics of the ion beam pulse are: singly-charged Cs^+ ions; ion energy $E_b=4$ GeV ($\beta_b=0.25$); maximum (in the middle section of the beam) ion current $I_b=4$ kA ($n_b=1.2\times10^{11}$ cm^{-3}); maximum beam radius $r_b=3$ cm; half-length $l_b=40$ cm; and background plasma density $n_p=10^{11}$ cm^{-3}. Shown in the figure are contour plots in $(z/l_b, r/r_b)$ space of: (a) ion density n_b in the beam pulse; (b) normalized longitudinal electron velocity V_{ez}/V_b; (c) normalized electron current $1-n_eV_{ez}/(N_bV_b)$, where $N_b\equiv n_b(0,0)$; (d) normalized longitudinal electric field E_z/E_{z0}, where $E_{z0}\equiv mV_b^2/(el_b)=410$ V/cm; (e) normalized radial electron velocity $V_{er}l_b/r_bV_b$; (f) normalized radial electric field in the beam E_r/E_{r0}, where $E_{r0}\equiv mV_b^2/(er_b)=5.467$ kV/cm; (g) normalized azimuthal magnetic-field B/B_0, where $B_0\equiv mcV_b/(er_b)=74G$; and (h) normalized radial force acting on the beam ions $(E_r-\beta_bB)/E_{r0}$, where $E_{r0}\equiv mV_b^2/(er_b)=5.467$ kV/cm.

return current and provide current neutrality. Therefore, the electric and magnetic fields also decrease with increasing plasma density. Figures 3(a) and 3(b) show that the radial force acting on the beam ions is less for small plasma density ($n_p<n_b$), compared to the case where $n_p\sim n_b$. This is because the radial electric field nearly compensates the self-magnetic force [$V_{ez}\simeq V_b$ in Eq. (21)]. For large plasma density ($n_p\gg n_b$), both the azimuthal magnetic field and the radial electric field are small due to the better current neutralization [Fig. 3(c)]. During ballistic focusing, the beam

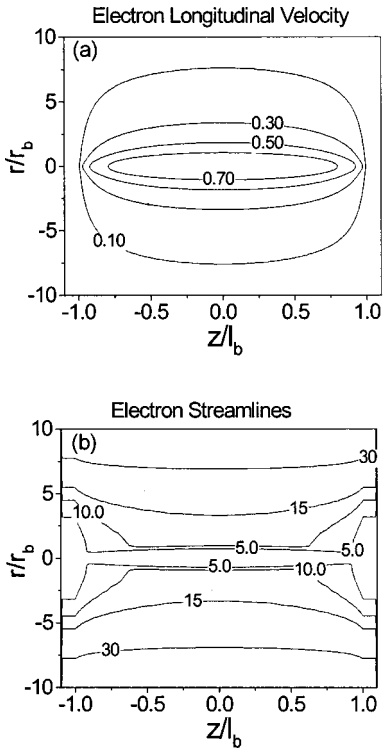

FIG. 2. Characteristics of the ion beam pulse are the same as in Fig. 1 but the background plasma density is $n_p=10^9\ \mathrm{cm}^{-3}$. Shown in the figure are contour plots in $(z/l_b, r/r_b)$ space of: (a) normalized longitudinal electron velocity V_{ez}/V_b; and (b) normalized integrated radial flux of electrons $\Gamma_z = \int_0^r [n_e(V_b - V_{ez}) - n_p V_b] r dr/(n_p V_b)$. The contour plots of Γ_z coincide with the electron trajectories in a frame moving with the beam.

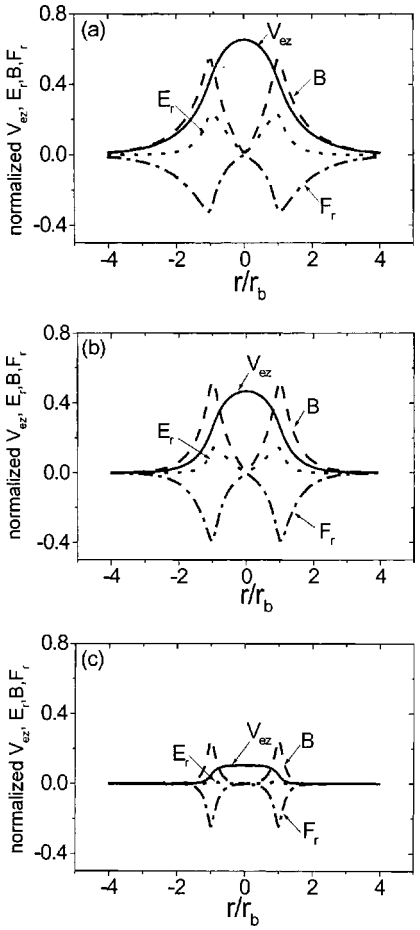

FIG. 3. Radial plots of the normalized electron velocity (V_{ez}/V_b), the radial electric field in the beam (E_z/E_{r0}), the azimuthal magnetic field in the beam (B/B_0), and the radial force acting on the beam ions $(E_r - \beta_b B)/(E_{r0})$, shown in the midplane of the ion pulse for the same conditions as in Fig. 1. The three plots correspond to plasma densities: (a) $n_p = 0.3\times 10^{11}\ \mathrm{cm}^{-3}$, (b) $n_p = 10^{11}\ \mathrm{cm}^{-3}$, (c) $n_p = 10^{12}\ \mathrm{cm}^{-3}$.

reduces in radius by about a factor of 10, and the radial electric field and azimuthal magnetic field increase by a similar factor, which follows from Eq. (17). An example of simulations for smaller beam radius is presented later in Fig. 7.

Figure 4 shows the degree of fractional charge nonneutralization, $f=\rho/(en_b)$, at the midplane of the beam for three values of the beam velocity. We have chosen parameters such that the departure from quasineutrality is approximately a maximum, corresponding to $r_b = c/\omega_b$, where $\omega_b^2 = 4\pi e^2 n_b/m_e$ is the electron plasma frequency calculated using the beam ion density. Moreover, a small plasma density with $n_p = 0.1 n_b$ is also assumed in Fig. 4. For the conditions in Fig. 4, the maximum value of f is about $0.2\beta_b^2$, which is much smaller than unity. Therefore, quasineutrality is very well satisfied.

C. Comparison of theoretical predictions with the results of electromagnetic particle-in-cell code

To check the theoretical predictions, we developed a two-dimensional (2D) electromagnetic particle-in-cell (PIC) code [for details see Ref. 16]. In developing this PIC code, we followed the approach of Morse and Nelson as given in Ref. 17. The code uses a leap-frog, finite-difference scheme[18] to solve Maxwell's equations (3) and (4) on a two-dimensional rectangular grid in the frame moving with the beam. The current deposition scheme is designed to conserve charge exactly,[17] so there is no need to solve Poisson's equation. Since the plasma ahead of the pulse is electrically neutral, the boundary condition for the fields on the front boundary are trivial $(\mathbf{E}=\mathbf{B}=0)$. The dynamics of the (stationary) background ions is neglected, and the plasma electrons are treated as cold. The beam ions are represented by a station-

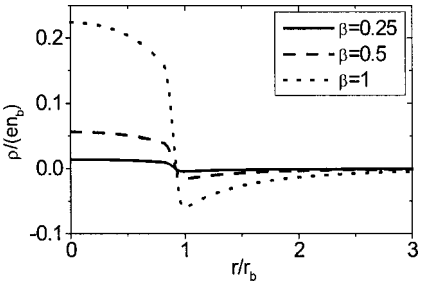

FIG. 4. Radial plots of the degree of fractional charge nonneutralization $f = \rho/(en_b)$ at the midplane of the ion beam pulse in background plasma assuming three values of beam velocity $\beta_b c$. The beam radius is chosen to be $r_b = c/\omega_b$, where $\omega_b^2 = 4\pi e^2 n_b/m_e$ is the electron plasma frequency squared calculated using the beam ion density. The beam radius chosen in the figure corresponds to the maximum degree of fractional charge nonneutralization. The corresponding beam current is $4.25\beta_b kA$, and the plasma density is $n_p = 0.1 n_b$.

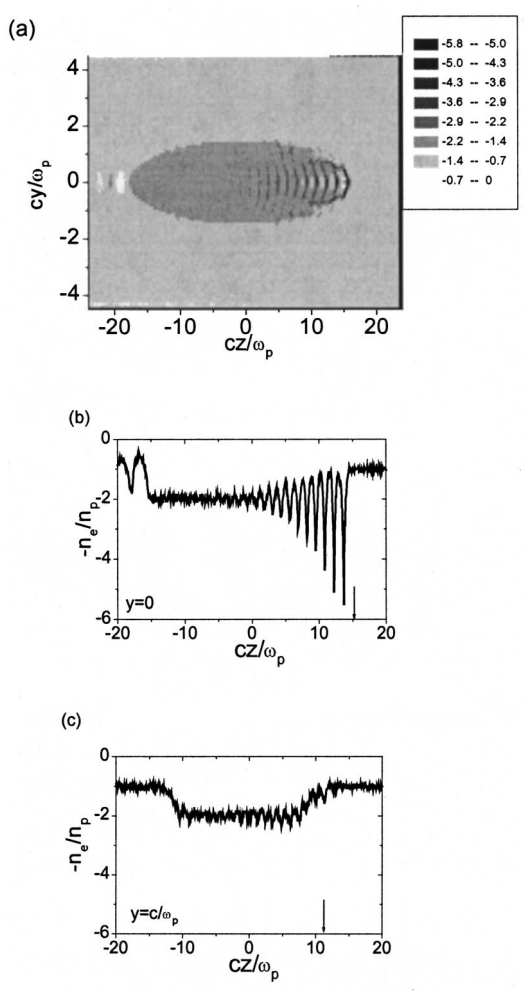

FIG. 5. The excitation of plasma waves by the beam head is calculated in two-dimensional slab geometry using the PIC-MC code (Ref. 25) for the following dimensionless beam parameters: $\beta_b=0.5$, $r_b=1.5c/\omega_p$, $l_b=15c/\omega_p$, $n_p=n_b$, and $Z_b=1$. Shown in the figure are (a) electron charge density contour plots in $(\omega_p z/c,\omega_p y/c)$ parameter space, and electron charge density vs $(\omega_p z/c)$ (b) for $y=0$ and (c) for $y=c/\omega_p$. The arrows show the beam edge.

ary (in the moving frame) current density on the simulation grid. To advance the electrons, we use the time-centered leap-frog scheme first introduced in Ref. 16.

Figures 5 and 6 show the results of self-consistent electromagnetic two-dimensional particle-in-cell (PIC) simulations in slab geometry. The simulation results in Fig. 5 show some phenomena associated with the finite neutralization length, neglected in the analytical theory, particularly the excitation of plasma waves by the beam front.

D. Generation of plasma waves by the beam edge

The sharp ion beam front excites plasma waves. In linear nonrelativistic theory, the plasma waves trail the beam front with period $l_p=2\pi V_b/\omega_p$, and the electron density is given by (see, for example, Ref. 4)

$$n_e(\zeta,y)-n_p=\int_{-\infty}^{\zeta}\sin\left(\frac{\omega_p}{V_b}(\zeta-\zeta')\right)n_b(\zeta',y)\,\frac{\omega_p}{V_b}\,d\zeta'. \tag{24}$$

Assuming a step-function profile for $n_b(\zeta',y)$, linear theory predicts electron density oscillations with amplitude n_b inside the beam, i.e.,

$$n_e(z,y)-n_p=\left[1-\cos\left(\frac{\omega_p}{V_b}(z_b(y)-z)\right)\right]n_b, \tag{25}$$

where $z_b(y)$ is the coordinate of the beam front. Figure 5(a) shows that the linear results are not valid, and the amplitude of oscillations can be as much as six times larger than the linear results. Nonlinear effects can also account for large increases in wave amplitude,[19] even in a cold plasma model. Indeed, in a one-dimensional model the nonlinear perturbation of the electron plasma density can be determined by combining Poisson's equation, total energy conservation, and the conservation of electron flux.[20] This gives

$$\frac{d^2\Phi}{d\zeta^2}=-4\pi e\left(n_b(\zeta)-\frac{n_0V_b}{\sqrt{V_b^2-2e\Phi/m}}\right). \tag{26}$$

Equation (26) describes nonlinear plasma oscillations and has no solution if Φ approaches $mV_b^2/2e$, where the electron density tends to infinity. For a step-function density profile for the beam ions, Eq. (26) can be solved analytically to give for the electric field $E=-d\Phi/d\zeta$,

$$E^2=8\pi e\int_0^{\Phi}\left(n_b-\frac{n_0V_b}{\sqrt{V_b^2-2e\Phi/m}}\right)d\Phi. \tag{27}$$

Ahead of the beam, the potential and electric field are zero; at the maximum of the electron density oscillation, the potential also has a maximum with $d\Phi/d\zeta=0$, and the electric field is zero. Therefore, the maximum potential in the plasma oscillation is given by

$$n_b\Phi_{\max}=\int_0^{\Phi_{\max}}\frac{n_0V_b}{\sqrt{V_b^2-2e\Phi/m}}\,d\Phi. \tag{28}$$

The singularity in electron density occurs when electrons are completely stopped by the potential barrier, i.e., the maximum potential energy $e\Phi_{\max}$ corresponds to $mV_b^2/2$. Making use of Eq. (28) one obtains that the condition $e\Phi_{\max}=mV_b^2/2$ occurs when

$$n_b=n_0. \tag{29}$$

Therefore, a step-function profile for the ion density with density equal or larger than the background plasma density induces large-amplitude plasma waves, which break and generate multiple electron flows, as observed in the simulations.

Figure 5 also shows the importance of two-dimensional effects. The linear result in Eq. (24) predicts that the plasma waves trail the beam front independently for any given y, and should not decay. Clearly, linear theory cannot predict the features of the plasma waves in Fig. 5, even qualitatively. The plasma waves in Fig. 5 do not repeat the beam edge form as predicted by the linear theory in Eq. (24), but have a different two-dimensional structure. Furthermore, the plasma waves are excited before the beam front at the radial edge of the beam [see Fig. 5(c)] and decay away from the front, in contrast to the predictions of linear theory. The accurate de-

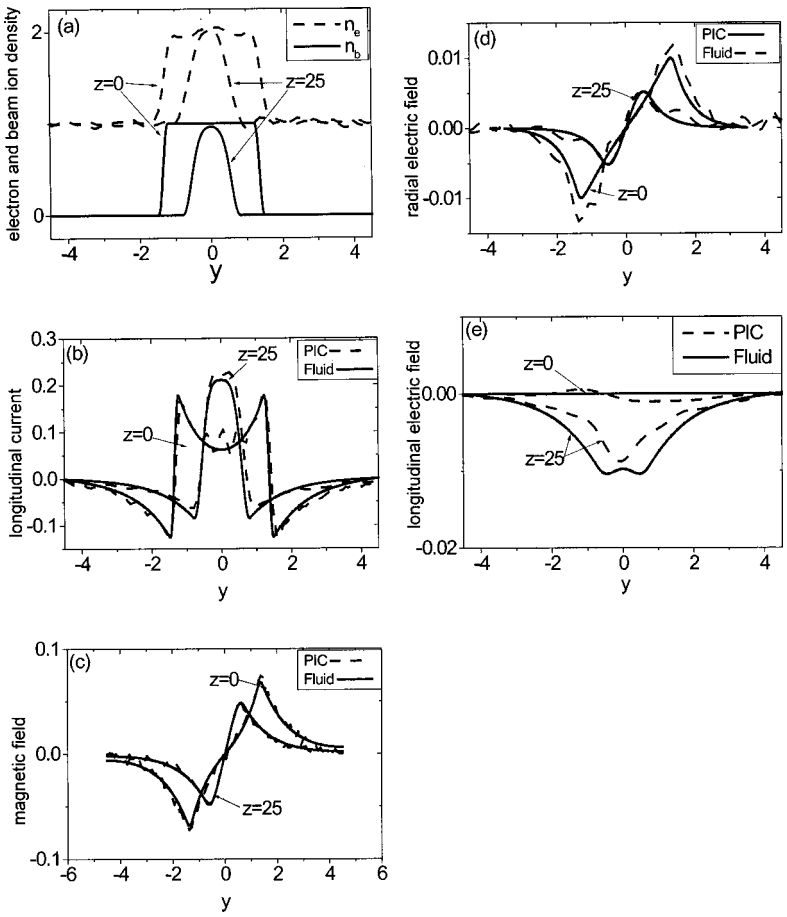

FIG. 6. Comparison of 2D particle-in-cell simulations with theoretical predictions for the following dimensionless parameters: $\beta_b=0.5$, $r_b=1.5c/\omega_p$, $l_b=30c/\omega_p$, and $n_p=n_b$ performed in two beam cross-sections: the midplane at $z=0$, and near the beam front at $z=25c/\omega_p$. The ion profile is smoothed according to Eq. (30), with $al_b=6c/\omega_p=(6/\pi)l_p$. Shown are radial plots of (a) normalized electron density n_e/n_p; (b) normalized longitudinal current $(n_bV_b-n_eV_{ez})/(n_pc)$; (c) normalized azimuthal magnetic field, $eB/(2m\omega_pc)$; (d) the normalized radial electric field $eE_r/(2m\omega_pc)$; and (e) normalized longitudinal electric field $eE_z/(2m\omega_pc)$.

scription of plasma wave excitation has to be performed using a nonlinear two-dimensional model and is beyond the scope of present paper.

To minimize the excitation of plasma waves, a smooth ion beam profile is used in the simulations shown in Fig. 6. We choose the profile

$$n_b(y,z)=n_{b0}\,f\left(\sqrt{\left(\frac{z}{l_b}\right)^2+\left(\frac{y}{r_b}\right)^2}\right), \tag{30}$$

where

$$f(s)=\begin{cases}0, & s>1,\\ g\left(\dfrac{1-s}{a}\right), & 1-a<s<1,\\ 1, & s<1-a.\end{cases} \tag{31}$$

Here, n_{b0} is the maximum beam density, $g(t)=10t^3-15t^4+6t^5$, and a is a parameter characterizing the width of profile smoothing. Plasma waves are not excited if the width of the beam front is much longer than the plasma period, i.e., $al_b\gg l_p$. For example, plasma waves are very weakly excited for the conditions chosen in Fig. 6, where $al_b=6l_p/\pi$, and the electron density is equal to the ion density within noise errors [Fig. 6(a)].

Figure 6 shows good agreement between results of the PIC simulations and the fluid calculations, both performed in slab geometry. The establishment of quasineutrality is clearly evident in Fig. 6(a). Small deviations from quasineutrality are due to numerical noise and excitation of plasma waves by the beam front. Figure 6(b) shows the difference in the current profile at two different beam cross sections. In the region of the beam head $(z=25c/\omega_p)$ the beam radius $r_b=1.6c/\omega_p$ is comparable to the skin depth, and correspondingly the electron current neutralizes about 80% of the ion current. In the midplane of the beam $(z=0)$, the beam radius $r_b=3c/\omega_p$ is larger than the skin depth, and correspondingly the electron current neutralizes more than 90% of the ion current in the beam center. The degree of current neutralization is smaller at the beam edge due to the sharp variation of the ion current profile. According to Eq. (12), the electron return current is a smooth decreasing function of radial coordinate r, and cannot neutralize (the nearly discontinuous) ion current. The magnetic field shows very good agreement between the analytical formulas [Eqs. (12) and (17)] and the PIC simulation results. The amplitude of the electric field is much smaller than the magnetic field. Therefore, the contributions due to numerical noise and plasma waves are more pronounced in Figs. 6(d) and 6(e) compared with Fig. 6(c). For the conditions in Fig. 6, the spatial resolution was 932×198 with nine particles per cell, which totals more than one and one-half million particles and requires a few hours of calculations on a one-processor Dell Pentium 1 GHz workstation. It is evident that an accurate calculation of the electric field using PIC simulations is very cumbersome in contrast with the semianalytical approach described above. In summary, the very good agreement of the electric and magnetic fields validates the proposed theory.

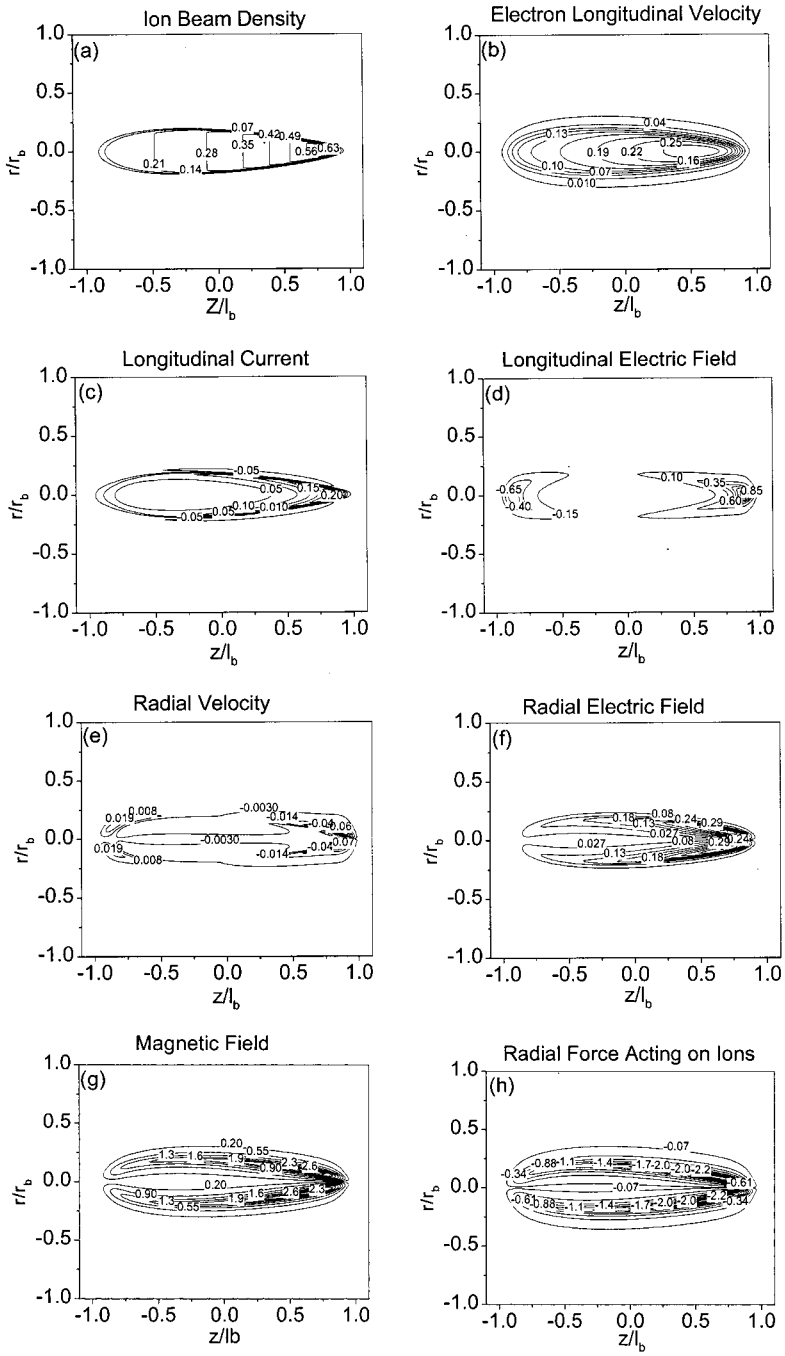

FIG. 7. Characteristics of a converging ion beam pulse. The figure labels and beam parameters are the same as in Fig. 1, except the unperturbed plasma density is $10^{13}\,\mathrm{cm}^{-3}$. The beam has propagated from a distance 5 m to a distance 1 m from the chamber center, ballistically converging to zero radius at the chamber center. Emittance effects and ion beam charge variations are neglected.

E. Converging ion beam

Figure 7 shows the results of simulations for a converging beam. The beam is assumed to be ballistically focused from its initial radius at the entrance to the chamber to zero radius at the chamber center, located at a distance 5 m from the chamber entrance. The initial beam parameters at the chamber entrance are taken to be the same as the parameters in Fig. 1. During ballistic focusing, neglecting the influence of self-fields on the beam ions, the beam ion trajectories are straight lines converging to the chamber center with mean radial velocity $V_{br}=V_{bz}r/Z_{ff}$, where Z_{ff} is the distance from the chamber center to the chamber entrance. For a cold ion beam, neglecting the radial ion thermal velocity, the beam density profile can be readily found to be[21]

$$n_b(r,z,t)=n_{b0}\frac{Z_{ff}^2}{z^2}f\left(r\frac{Z_{ff}}{z},z-Z_{\mathrm{center}}(t)\right), \tag{32}$$

where z is the distance from chamber center, $Z_{\mathrm{center}}(t)$ is the position of the beam center, and $f(r,z)$ is the initial beam density profile in Eq. (31). The ion beam density profile for $Z_{\mathrm{center}}(t)=1$ m is shown in Fig. 7(a). Ion beam charge variation effects due to possible beam ion ionization have been neglected ($Z_b=1$). As can be seen from the figure, the beam radius is reduced approximately by a factor of five times

compared with Fig. 1, and the beam density is peaked in the beam head region. The background electron density in Fig. 7 has been increased by a factor of one hundred compared with Fig. 1, with $n_p = 10^{13}\,\mathrm{cm}^{-3}$. This high value of plasma density is assumed at distances close to the target because of gas photoionization produced by the ''foot'' prepulse striking the fusion pellet, producing large amount of radiation at earlier times.[22] The electron longitudinal flow velocity obtained from Eq. (12) is shown in Fig. 7(b). The corresponding skin depth, $c/\omega_p = 0.17\,\mathrm{cm}$, is comparable to the beam radius in the beam center and larger than the beam radius in the beam head. Therefore, the ion current is neutralized in the beam center and is not neutralized in the beam head. Correspondingly, the magnetic field [Eq. (6)] in the beam head is much larger than in the beam tail [see Fig. 7(g)]. The electric field is calculated from Eq. (7) and depicted in Figs. 7(d) and 7(f). The radial electron flow velocity shown in Fig. 7(e) is more negative compared with the steady-state situation in Fig. 1(e) due to the beam convergence [compare Eqs. (23) and (15)]. The charge neutralization estimated from Eq. (18) is close to unity, i.e., about 98%. As evident from Fig. 7(h), the radial force acting on the beam ions is a maximum at the beam edge and in the front part of the beam.

V. CONCLUSIONS AND OUTLOOK

The propagation of a finite-length ion beam pulse through a uniform, stationary background plasma has been studied. The analytical solutions for the electric and magnetic fields generated by an ion beam pulse have been determined in the nonlinear case for arbitrary values of n_p/n_b under the assumption of a long beam, where the beam length is much longer than the beam radius and the plasma neutralization length (V_b/ω_b). Under these conditions, a reduction in the dimensionality of the problem is possible. Assuming an axisymmetric beam, the longitudinal electron flow velocity is determined for one-dimensional variations in the radial direction for each axial slice of the beam. The electric and magnetic fields are then readily calculated from the longitudinal electron flow velocity. As a result, numerical simulations are very fast, even for very long beams with a large ratio of the beam length to the beam radius. Since the electron response time is much faster than the ion beam pulse duration, any variations in plasma or beam parameters are adiabatically slow on the electron time scale. The approach used here can be generalized to the case of nonuniform nonstationary plasma density and beam density profiles, and forms the basis for a hybrid semianalytical approach to be used for calculations of beam propagation in the target chamber. This work is now underway.

The assumption of zero generalized vorticity can be broken if plasma is generated inside the beam, where the magnetic field is not zero. Therefore, if a considerable amount of plasma is produced by beam ionization processes, the approach presented here requires modification.

The assumption of immobile background ions can be incorrect for very long beams. Indeed, the radial displacement of a plasma ion with mass m_i during the beam pulse duration $2l_b/V_b$ caused by the radial electric field in Eq. (16) [which at maximum is of order $mV_b^2/(er_b)$] is larger than the beam radius whenever $(m/m_i)(2l_b/r_b)^2 > 1$. For the beam parameters considered for heavy ion fusion, the beam aspect ratio (l_b/r_b) is less than one hundred, and the background ion dynamics can be neglected for all gases, except possibly for hydrogen.

The analytical formulas derived in this paper can provide an important benchmark for numerical codes and provide scaling laws for different beam and plasma parameters. The simulations of current and charge neutralization performed for conditions relevant to heavy ion fusion typically showed very good charge neutralization and considerable current neutralization. Moreover, an important conclusion of the present analysis is that for long, dense beams (length $l_b \gg V_b/\omega_b$, where V_b is the beam velocity, and ω_b is the electron plasma frequency evaluated with the ion beam density), the charge neutralization is very good even for a tenuous background plasma with density much smaller than the beam density. The background plasma is collected radially over the distances of order the electron skin depth, and the small value of plasma density can be well compensated by the large dimension of the collecting region.

ACKNOWLEDGMENTS

This research was supported by the U.S. Department of Energy Office of Fusion Energy Sciences and Division of High Energy Physics.

It is a pleasure to acknowledge the benefit of useful discussions with Ed Lee, Marshall Rosenbluth, and Wei-li Lee.

APPENDIX A: ELECTROSTATIC AND VECTOR POTENTIALS

In the present work we have attempted to avoid using specific gauges and expressed all results in terms of the electric field $\mathbf{E} = -\nabla\phi - \mathbf{c}^{-1}\partial\mathbf{A}/\partial t$ and the magnetic field $\mathbf{B} = \nabla\times\mathbf{A}$. Since a number of authors find it convenient to use the scalar and vector potentials, ϕ and $\mathbf{A}$, we list here for completeness some of the popular gauges, and also introduce a new gauge, which is, in our opinion, well suited for the problem at hand. Examples of the gauges used in the literature include the Coulomb gauge, $\nabla\cdot\mathbf{A} = 0$, the transverse Coulomb gauge, $\nabla_\perp\cdot\mathbf{A}_\perp = 0$, and the Arnowitt–Fickler relativistically covariant gauge, $A_\mu n^\mu = 0$, where A_μ is the 4D vector potential, and $\mathbf{n}$ is any 4D vector, e.g., the 4D momentum p^μ can be used as $\mathbf{n}$.[23] If we choose p^μ as the momentum of the plasma ions, then the Arnowitt–Fickler gauge reduces to zero electrostatic potential, $\varphi = 0$. Even more elaborate gauges designed to cancel specific terms in Maxwell's equations have been proposed in Ref. 3.

Equation (7) suggests that a natural choice of gauge is

$$e\phi = K_e, \tag{A1}$$

which gives

$$\frac{e}{c}\mathbf{A} = \mathbf{p}_e. \tag{A2}$$

All other gauges imply that the vector potential $\mathbf{A}$ would differ from the momentum $c\mathbf{p}_e/e$ by the gradient of an arbi-

trary function [Eq. (6)]. For example, in the present analysis, the full Coulomb gauge is not convenient because of the necessity to make the vector potential divergence free, $\nabla \cdot \mathbf{A}=0$.

For cylindrically symmetric beams, it is convenient to use the transverse Coulomb gauge, $\nabla_\perp \cdot \mathbf{A}_\perp = 0$. In cylindrical geometry, assuming axisymmetry in the azimuthal direction, it follows that $\mathbf{A}_\perp = 0$, and the fields are completely described by the electrostatic potential ϕ, and the z component of the vector potential $\mathbf{A}=A_z\hat{\mathbf{e}}_z$, where $\hat{\mathbf{e}}_z$ is a unit vector along the z axis. Therefore, the fields can be expressed as

$$\mathbf{B}=\nabla A_z \times \hat{\mathbf{e}}_z, \quad \mathbf{E}=-\nabla\phi-\frac{1}{c}\frac{\partial A_z}{\partial t}\hat{\mathbf{e}}_z. \tag{A3}$$

Integration of the London equation (6) gives an explicit equation for the vector potential

$$\frac{e}{c}A_z\hat{\mathbf{e}}_z=\mathbf{p}_e-\nabla\varkappa, \tag{A4}$$

where $\varkappa$ is an unknown function. From the radial component of Eq. (A4) it follows that

$$\varkappa(\zeta,r)=-\int_r^\infty p_{er}dr,$$

and the longitudinal component of the vector potential can be expressed as

$$\frac{e}{c}A_z=p_{ez}+\frac{\partial\varkappa}{\partial\zeta}. \tag{A5}$$

Finally, the electrostatic potential ϕ can be determined by integrating the radial component of Eq. (7), which gives

$$e\phi=K_e+V_b\frac{\partial\varkappa}{\partial\zeta}. \tag{A6}$$

The use of any particular gauge does not really simplify the problem. We have listed them here for reference only.

APPENDIX B: CONSERVATION OF THE GENERALIZED VORTICITY

The success of the analytical solution for the nonlinear charge and current neutralization of an ion beam pulse in a pre-formed plasma relies heavily on the London equation (6), which is based on the assumption of zero generalized vorticity. In this appendix we give a detail proof of the condition for validity of this assumption.

Equation (5) for the generalized vorticity $\mathbf{\Omega}$ can be expressed as

$$\frac{\partial\mathbf{\Omega}}{\partial t}+(\mathbf{V_e}\cdot\nabla)\mathbf{\Omega}=-\mathbf{\Omega}(\nabla\cdot\mathbf{V_e})+(\mathbf{\Omega}\cdot\nabla)\mathbf{V}_e. \tag{B1}$$

Equation (B1) shows that the generalized vorticity is transported along with the electrons and that the source term on the right-hand side is proportional to the generalized vorticity. Therefore, if the generalized vorticity $\mathbf{\Omega}$ is initially equal to zero everywhere, then it remains equal to zero everywhere. To elaborate further we include another derivation, similar to the analysis performed in hydrodynamics in Ref. 26. Consider the circulation C of the canonical momentum

$$C\equiv\oint(\mathbf{p}_e-e\mathbf{A}/c)\cdot\delta\mathbf{r}, \tag{B2}$$

taken along a closed loop, where $\mathbf{A}$ is the vector potential, and $\mathbf{B}=\nabla\times\mathbf{A}$ is the magnetic field. We shall consider the loop as ''frozen-in,'' moving together with the electron fluid. The evolution of the circulation of the canonical momentum is determined by its full derivative

$$\frac{dC}{dt}\equiv\frac{d}{dt}\oint(\mathbf{p}_e-e\mathbf{A}/c)\cdot\delta\mathbf{r}. \tag{B3}$$

The full derivative accounts for the fact that the contour position is changing. Application of the chain rule results in

$$\frac{dC}{dt}=\oint\frac{d}{dt}(\mathbf{p}_e-e\mathbf{A}/c)\cdot\delta\mathbf{r}+\oint(\mathbf{p}_e-e\mathbf{A}/c)\cdot\frac{d}{dt}\delta\mathbf{r}. \tag{B4}$$

Substituting $d\delta\mathbf{r}/dt=\delta\mathbf{V}_e$ and using Eq. (2) gives

$$\frac{dC}{dt}=\oint\frac{e}{c}[c\nabla\phi-\mathbf{V}_e\times(\nabla\times\mathbf{A})-(\mathbf{V}_e\cdot\nabla)\mathbf{A}]\cdot\delta\mathbf{r}+\oint(\mathbf{p}_e-e\mathbf{A}/c)\cdot\delta\mathbf{V}_e. \tag{B5}$$

Rewriting $\delta\mathbf{V}_e=(\delta\mathbf{r}\cdot\nabla)\mathbf{V}_e$, we express

$$\delta\mathbf{r}\cdot(\nabla\mathbf{V}_e)\cdot\mathbf{A}=\delta\mathbf{r}\cdot[\mathbf{A}\times(\nabla\times\mathbf{V_e})+(\mathbf{A}\cdot\nabla)\mathbf{V_e}]. \tag{B6}$$

Substituting this expression into Eq. (B5) and rearranging terms yields

$$\frac{dC}{dt}=\oint\frac{e}{c}[c\nabla\phi-\nabla(\mathbf{V_e}\cdot\mathbf{A})]\cdot\delta\mathbf{r}+\oint\mathbf{p}_e\cdot\delta\mathbf{V}_e. \tag{B7}$$

All integrals in Eq. (B7) are equal to zero for closed contours, since the integral over a gradient is equal to zero for closed contours, and the last integral on the right-hand side of Eq. (B7) is an integral over the differential function $L(\mathbf{p}_e)\mathbf{p}_e\cdot\delta\mathbf{V}_e=\delta L(\mathbf{p}_e)$, where $L(\mathbf{p})=\mathbf{p}_e\cdot\mathbf{V}_e-K_e$. Therefore, the circulation of the canonical momentum is conserved, i.e., $dC/dt=0$.

Applying Thompson's theorem, the circulation defined in Eq. (B2) can be rewritten as the surface integral of the generalized vorticity

$$C=\oint(\mathbf{p}_e-e\mathbf{A}/c)\cdot\delta\mathbf{r}=\int\nabla\times(\mathbf{p}_e-e\mathbf{A}/c)\cdot\delta\mathbf{S}\equiv\int\Omega\cdot\delta\mathbf{S}, \tag{B8}$$

where $\delta\mathbf{S}$ is the fluid surface element. Note that because $\int\mathbf{\Omega}\cdot\delta\mathbf{S}=$ constant, the terms on the right-hand side of Eq. (B1) describe the distortion of the fluid surface element $\delta\mathbf{S}$. Because $dC/dt=0$, the circulation C is conserved along electron streamlines. Therefore, the condition $\mathbf{\Omega}=0$ is preserved on the streamlines, and if $\mathbf{\Omega}=0$ everywhere initially, then $\mathbf{\Omega}$ remains equal to zero everywhere at subsequent times.

It is possible to perform an even simpler proof by making use of the fact that the integral of the Lorentz force over the frozen-in contour is equal to the full derivative of the magnetic flux[24]

$$\oint \left(\mathbf{E} + \frac{1}{c} \mathbf{V}_e \times \mathbf{B}_e \right) \cdot \delta \mathbf{r} = \frac{1}{c} \frac{d}{dt} \int \mathbf{B} \cdot \delta \mathbf{S}. \tag{B9}$$

Equation (B9) immediately yields

$$\frac{d}{dt} \oint \mathbf{p}_e \cdot \delta \mathbf{r} = \frac{e}{c} \frac{d}{dt} \int \mathbf{B} \cdot \delta \mathbf{S}, \tag{B10}$$

and consequently equation $dC/dt = 0$ follows directly.

[1] H. Alfven, Phys. Rev. **55**, 425 (1939).
[2] W. H. Bennett, Phys. Rev. **45**, 890 (1934).
[3] D. A. Hammer and N. Rostoker, Phys. Fluids **13**, 1831 (1970); J. L. Cox and W. H. Bennett, *ibid.* **13**, 182 (1970).
[4] P. Chen, J. M. Dawson, R. W. Huff, and T. Katsouleas, Phys. Rev. Lett. **54**, 693 (1985).
[5] P. Chen, Part. Accel. **20**, 171 (1987); P. Chen, J. J. Su, T. Katsouleas, S. Qilks, and J. M. Dawson, IEEE Trans. Plasma Sci. **PS-15**, 218 (1987).
[6] R. Govil, W. P. Leemans, E. Yu. Backhaus, and J. S. Wurtele, Phys. Rev. Lett. **83**, 3202 (1999); G. Hairapetian, P. Davis, C. E. Clayton, C. Joshi, S. C. Hartman, C. Pellegrini, and T. Katsouleas, *ibid.* **72**, 2403 (1994).
[7] M. Roth, T. E. Cowan, M. H. Key *et al.*, Phys. Rev. Lett. **86**, 436 (2001); M. Tabak, J. Hammer, M. E. Glinsky, W. L. Kruer, S. C. Wilks, J. Woodworth, E. M. Campbell, M. D. Perry, and R. J. Mason, Phys. Plasmas **1**, 1626 (1994).
[8] K. Hahn and E. P. Lee, J. Fusion Energy **32–33**, 417 (1996).
[9] S. Rajagopalan, D. B. Cline, and P. Chen, Nucl. Instrum. Methods Phys. Res. A **355**, 169 (1995); J. S. T. Ng, P. Chen, H. A. Baldis *et al.*, "Results on plasma focusing of high energy density electron and positron beams," Invited talk presented at the 9th Workshop on Advanced Accelerator Concepts, Santa Fe, New Mexico, June 11–16, 2000; SLAC-PUB-8565, August 2000.
[10] T. Tauschwitz, S. S. Yu, S. Eylon, L. Reginato, W. Leemans, J. O. Rasmussen, and R. O. Bangerter, J. Fusion Energy **32–33**, 493 (1996).
[11] B. N. Breizman, D. L. Fisher, P. Z. Chebotaev, and T. Tajima, "Excitation of nonlinear wake field in a plasma for particle acceleration," in *Research Trends in Physics: Coherent Radiation Generation and Particle Acceleration*, edited by A. M. Prokhorov (American Institute of Physics, New York, 1992), p. 263, and IFS report #502 (1992); J. B. Rozenzweig, D. B. Cline, H. Figueroa, W. Gai, R. Wonecny, J. Norem, P. Schoessow, and G. Simpson, Phys. Rev. Lett. **61**, 98 (1988); J. B. Rosenzweig, B. N. Breizman, T. Katsouleas, and J. J. Su, Phys. Rev. A **44**, R6189 (1991).
[12] M. Rosenbluth, E. P. Lee and R. Briggs, private communication (2001).
[13] W. Lee, H. Qin, and R. Davidson, *Proceedings of the International Symposium on Heavy Ion Fusion*, San Diego (2000), in Nucl. Instrum. Methods Phys. Res. A **464**, 465 (2001).
[14] L. M. Gorbunov, Sov. Phys. Usp. **16**, 217 (1973).
[15] D. D.-M. Ho, S. T. Brandon, and E. P. Lee, Part. Accel. **35**, 15 (1991).
[16] J. P. Boris and K. V. Roberts, J. Comput. Phys. **4**, 552 (1969).
[17] R. L. Morse and C. W. Nielson, Phys. Fluids **14**, 830 (1971).
[18] C. K. Birdsall and A. B. Langdon, *Plasma Physics via Computer Simulations*, 2nd ed. (Plenum, New York, 1984).
[19] R. C. Davidson, *Methods in Nonlinear Plasma Theory* (Academic, New York, 1972), p. 39.
[20] A. I. Akhiezer and R. V. Polovin, Sov. Phys. JETP **3**, 696 (1956).
[21] E. P. Lee, S. Yu, H. L. Buchanan, F. W. Chambers, and M. N. Rosenbluth, Phys. Fluids **23**, 2095 (1980).
[22] W. M. Sharp and B. G. Logan, private communication (2001).
[23] P. Ramond, *Field Theory: A Modern Primer* (Addison-Wesley, Reading, MA, 1990).
[24] L. D. Landau and E. M. Lifshitz, *Electrodynamics of Continuous Media*, 2nd ed. (Pergamon, Oxford, 1993), Chap. VII, Sec. 63.
[25] E. A. Startsev and C. J. McKinstrie, "Particle-in-cell simulations of ponderomotive particle acceleration in a plasma," Phys. Rev. E (to be published).
[26] L. D. Landau and E. M. Lifshitz, *Fluid Mechanics*, 2nd. ed. (Butterworth-Heinemann, Oxford, 1997).